ELSEVIER

Chemical Engineering Journal 72 (1999) 217–227

Chemical Engineering Journal

Studies of local heat transfer in a gas–liquid system agitated by double disc turbines in a slender vessel

Joanna Karcz

Technical University of Szczecin Al. Piastów 42, 71-065, Szczecin, Poland

Received 6 November 1997; received in revised form 17 July 1998; accepted 16 November 1998

Abstract

In the paper, experimental studies of the distributions of heat transfer coefficient along the wall of the slender agitated vessel equipped with a dual Rushton turbine system are presented. Thermal measurements for liquid and gas–liquid system were carried out by means of the special heat flux meter. The agitated vessel of inner diameter D=0.3 m, filled with liquid up to height H=2D was used in the studies. The profiles of the heat transfer coefficient were obtained for different superficial gas velocities and impeller speed within the turbulent regime of the fluid flow. The distributions were approximated by Eqs. (25)–(30) and compared with the analogous profiles obtained for the system with the single disc turbine.

Keywords: Agitation; Heat transfer; Gas–liquid system; Local heat transfer coefficient

1. Introduction

Agitation of liquids and gas–liquid systems in the agitated vessels is a common unit operation in the chemical and biochemical industries. Mass transfer process in such systems should be often carried out at conditions of the exactly determined temperature, then the control of the heat transferred through the heating/cooling coil or jacket mounted in the vessel will be required.

Heat transfer coefficient α at the wall of the agitated vessel depends on the many factors, such as type and geometry of the vessel and agitator, physical parameters of the agitated system and operating variables. The coefficient α depends also on the position at the heat transfer surface, therefore the distributions of α at the agitated vessel wall can be found.

The investigations of the local heat transfer coefficient α_l are described in the literature [1–16,18,20], but the results for gas–liquid system are presented in a few papers [6,9–14,20] only. The measurements of the heat transfer process are usually carried out by means of the thermal method, but other measuring methods based on the analogy of mass and heat transfer processes (for example, electrochemical method) are also adopted in the studies. Different types of the local measuring elements were used for the measurements: special heat flux meters [1,5,9–12,18], electrochemical sensors [2,3,14,15,20], micro foil sensors [4,6–8] or thermister probes [13].

The limiting effects caused by the developing of the temperature profile in the liquid laminar boundary layer can complicate the measurements of local heat transfer coefficient, which are conducted using the small sensors. If the size of such a sensor is considered as insufficient to eliminate the limiting effect then the result of the measurement can be corrected by means of the experimentally determined calibration factor p.

In the papers [1,5,9,10,18], the distributions of the local heat transfer coefficients α_l along the wall of the agitated vessel were determined from direct measurements of the heat flux q_w and difference of temperature ΔT_l between wall temperature T_w and liquid temperature T_m. Bourne et al. [2,3], Man et al. [14,15] and Stręk et al. [20] used in the studies an electrochemical method in which the diffusion current is measured and local heat transfer coefficients are calculated from analogy of the mass and heat transfer data. Platzer and Noll [16] evaluated the distributions of the coefficient α_l on the basis of Colburn analogy between momentum and heat transfer.

Haam et al. [6] used the heat flow sensors and PC data acquisition system for the study of local heat transfer in a gas–liquid system agitated by single Rushton impeller in a baffled vessel of inner diameter D=0.387 m. They measured the variation of the local coefficients with angular position

1385-8947/99/$ – see front matter
PII: S1385-8947(99)00005-4

on the vessel wall, especially in the regions close to baffles, within the range of the agitator speed n (s^{-1})$\in\langle 3.33;\ 14.2\rangle$ and superficial gas velocity w_{og} (m s^{-1})$\in\langle 3\times10^{-3};\ 5\times10^{-2}\rangle$. The results of the thermal measurements were approximated by means of the function $Nu_l=f(Re,\ Pr,\ Vi,\ w_{og}/nd)$, where introduced a gas flow dimensionless number w_{og}/nd was used, that improved significantly the correlation for the single impeller.

Analysing the profiles of the coefficient α_l obtained for gas–liquid system agitated in the standard vessel of inner diameter D=0.3 m, Man [14] proved that mean heat transfer coefficients decrease about 15% in comparison with the results for the liquid phase. As literature data show, problems of the local heat transfer occurring in the gas–liquid systems produced in the agitated vessels of nonstandard geometry have not been studied sufficiently, yet.

The purpose of the experimental study was to investigate the distributions of the heat transfer coefficient at the wall of the slender agitated vessel equipped with a dual Rushton turbine system. The thermal measurements for liquid and gas–liquid system were carried out by means of the special heat flux meter.

2. Estimation of an effect of the size of the heat flux meter on local heat transfer coefficient

Local heat transfer coefficient α_l can be calculated from equation

$$\alpha_l = \frac{dQ_l}{\Delta T_l \cdot dF} = \frac{q_w}{\Delta T_l}, \tag{1}$$

where index w refers to the wall (y=0). In the zone of the local heat source, profile of the temperature within thermal boundary layer has been forming, yet. Namely, part of the heat transferred from the wall to the liquid is accumulated in the boundary layer, and other part of the heat is transported to the turbulent stream of the liquid. Heat balance for two-dimensional fluid element $dy\,dz$ in the vicinity of the wall illustrates Fig. 1(a). As Fig. 1(b) shows, the heat flux q_w decreases and reaches the value $q_{w,z\to\infty}$ for the $z\to\infty$.

Introducing the correction factor p defined as

$$p = \frac{q_{w,z\to\infty}}{q_{w,z}}, \tag{2}$$

where $q_{w,z}$ is the heat flux measured in the point of z coordinate, $q_{w,z\to\infty}$ is the heat flux for the completely formed thermal boundary layer, i.e. $z\to\infty$, an effect of the noncompletely formed thermal boundary layer on the local heat transfer coefficient can be taken into account in the calculations. Rearranging definition (2)

$$p = \frac{q_{w,z\to\infty}}{q_{w,z}} = \left(\frac{-\lambda(\partial T/\partial y)_{z\to\infty}}{-\lambda(\partial T/\partial y)_z}\right)_{y=0}, \tag{3}$$

we obtain the equation

$$p = \frac{\left.\frac{\partial T}{\partial y}\right|_{y=0;z\to\infty}}{\left.\frac{\partial T}{\partial y}\right|_{y=0;z}}. \tag{4}$$

As the heat flux is measured in the point z=R by means of the circular local heat source with a diameter of 2R then correction factor p is determined by

$$p = \frac{\left.\frac{\partial T}{\partial y}\right|_{y=0;z\to\infty}}{\left.\frac{\partial T}{\partial y}\right|_{y=0;z=R}}. \tag{5}$$

Assuming identical driving difference of temperature, correction factor p can be used for the calculation of the coefficient α_l because

$$q_w = \alpha_l \cdot \Delta T_l, \tag{6}$$

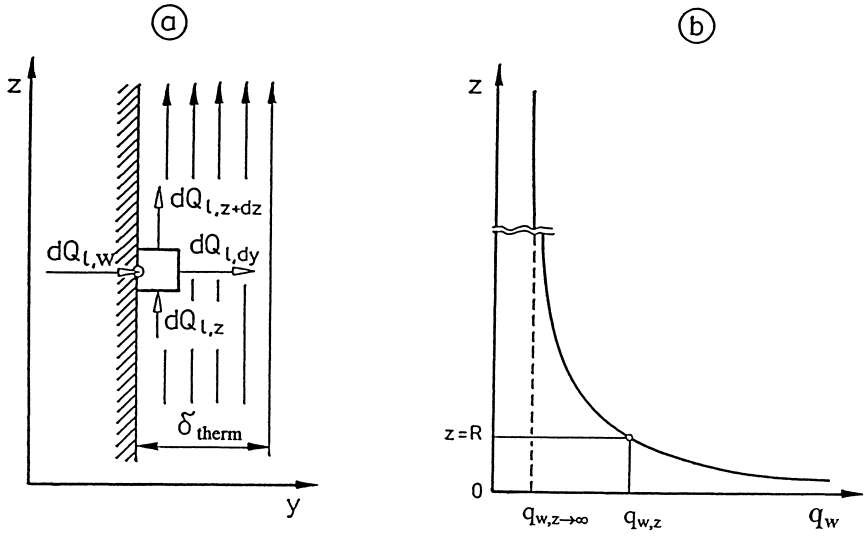

Fig. 1. Region of the formation of thermal boundary layer. (a) thermal balance for liquid element $dy\,dz$; (b) distribution of the heat flux q_w.

therefore

$$p = \frac{q_{w,z\to\infty}}{q_{w,z=R}} = \frac{\alpha_{l,z\to\infty}}{\alpha_{l,z=R}}. \quad (7)$$

In fact, analysed model describes the heat flux meter with the rectangular cross-section, however it can be used in the case of the meter with circular cross-section when heat flux q_w is measured in the point $z=R$.

Distribution of the temperature within two-dimensional thermal boundary layer describes differential equation

$$w_z \frac{\partial T}{\partial z} = a \frac{\partial^2 T}{\partial y^2}. \quad (8)$$

Assuming the Eq. (8) linear relationship of the axial velocity w_z on the coordinate y

$$w_z = c \cdot y = \gamma \cdot y, \quad (9)$$

where γ (s^{-1}) denotes shear rate, we obtain the following equation

$$\gamma \cdot y \frac{\partial T}{\partial z} = a \frac{\partial^2 T}{\partial y^2}. \quad (10)$$

which should be solved with the following boundary conditions

$$T = T_w \quad \text{for } y = 0,$$
$$T = T_m \quad \text{for } y = \delta_t. \quad (11)$$

The temperatures within nodes of the rectangular grid, shown in Fig. 2, can be found from the numerical computations of Eq. (10). Assuming that

$$T_w = T_{1,0} = \cdots = T_{k,0} = \cdots = T_{n,0}, \quad (12)$$
$$T_m = T_{1,m} = \cdots = T_{j,m} = \cdots = T_{n,m}. \quad (13)$$
$$T_w > T_m,$$

the correction factor p according to Eq. (7) will be defined as

$$p = \frac{(T_{n,0} - T_{n,m})/m}{T_{k,0} - T_{k,1}} = \frac{(T_w - T_m)/m}{T_w - T_{k,1}}. \quad (14)$$

In the $k+1$, j node of the grid the temperature is determined from the following equation:

$$T_{k+1,j} = T_{k,j} + dT_{k,j} = T_{k,j} + \frac{A_{k,j}}{j}[T_{k,j+1} - 2T_{k,j} + T_{k,j-1}], \quad (15)$$

where

$$A_{k,j} = \frac{a}{dy^2} \cdot \frac{1}{\gamma_{k,j}} \cdot \frac{dz}{dy} = \frac{\nu}{Pr \cdot \gamma_{k,j}} \cdot \frac{dz}{dy^3}. \quad (16)$$

In general, $\gamma_{k,j}$ depends on the temperature because liquid viscosity in the boundary layer changes with the temperature.

Some results of the calculations of the factor p as a function of the heat source size R (in general, linear dimension z) are given in Fig. 3. Curves 1 and 2 were obtained for distilled water, assuming: (1) α_1=1000 and α_2=600 W m^{-2} K^{-1}, then thickness $\delta_{t1}=\lambda/\alpha=6\times10^{-4}$ m and $\delta_{t2}=10^{-3}$ m, respectively; (2) in both cases γ=150 1 s^{-1} at the wall, then velocities $W_{z,1}=\gamma\delta_{t,1}=9\times10^{-2}$ m s^{-1} and $W_{z,2}$=0.15 m s^{-1}, respectively. The calculations were carried out for other parameters Pr_1=7.06; $\nu_1=10^{-6}$ m^2 s^{-1} ($\eta_1=10^{-3}$ kg ms^{-1}); m=20; $dz\leq10^{-5}$. The results for 25% and 50% aqueous solutions of glycerol, illustrated by curves 3 and 4, were obtained for the following data: $\nu_3=10^{-6}$ m^2 s^{-1} ($\eta_3=10^{-3}$ kg ms^{-1}); $\nu_4=10^{-6}$ m^2 s^{-1} ($\eta_4=10^{-3}$ kg ms^{-1}); Pr_3=14; Pr_4=42; in both cases $\delta_t=10^{-3}$ m; γ=150 s^{-1}; m=20; $dz=10^{-5}$. As numerical data in Fig. 3 show, correc-

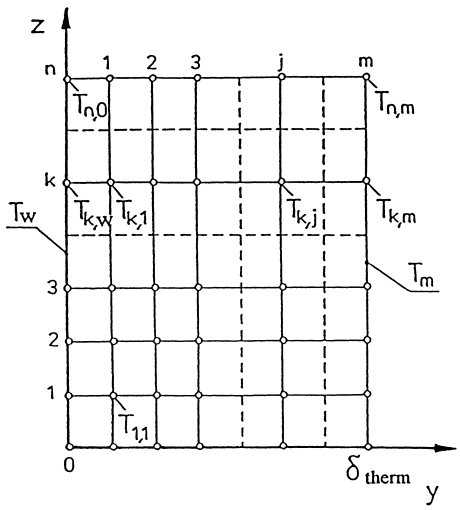

Fig. 2. Nodes of the rectangular grid.

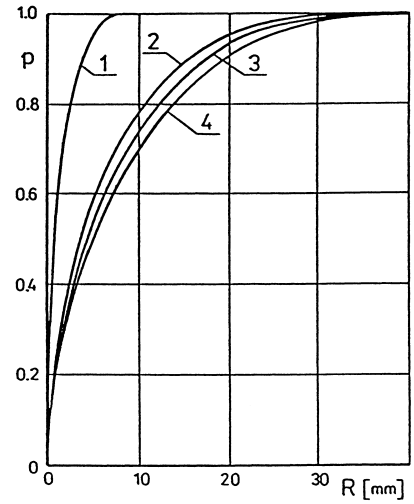

Fig. 3. The dependence of the correction factor p on the radius R of the thermal measuring element. (a) Distilled water, $\delta_{therm}=6\cdot10^{-4}$ m; (b) distilled water, $\delta_{therm}=10^{-3}$ m; (c) 25% aqueous solution of glycerol, $\delta_{therm}=10^{-3}$ m; (d) 50% aqueous solution of glycerol, $\delta_{therm}=10^{-3}$ m.

tion factor $p \approx 1$ for the dimension of the heat source $R=30$ mm, within wide range of the liquid viscosity.

3. Experimental

Experiments were carried out in a slender agitated vessel equipped with flat bottom, baffles and one or two Rushton disc turbines. Geometrical parameters of the agitated vessel used in the study are specified in Fig. 4 and Table 1.

Experimental set-up is shown in Fig. 5. Agitated vessel (1) equipped with baffles (2) was made of organic glass of thickness 6 mm and consisted of the segments of different height which were selected in such a way that the location of a heat source (3) in the wall was possible at various distances from the bottom of the vessel. Disc turbines (5) were driven by an electric motor (6) coupled with steering unit (7). Impeller speeds, determined by means of a photoelectric method, were measured using a digital counter (8). Air fed via control valve (10) and a rotameter (11) was dispersed in the agitated vessel by gas sparger in the form of a ring (9) of diameter $d_d=0.7d$ and with six 2 mm holes symmetrically placed on the perimeter.

Local heat source (3) [19] was heated by the steam of temperature approximately 102°C. A manometer (13) and thermometer (14) were used to control the pressure and temperature of the steam. The condensate was collected in the condenser pot (15). The values of the thermal electromotive force from thermocouples (16) built in the heat source were recorded by point recorder (18).

Table 1
Geometrical parameters of the agitated vessel, used in the study

No.	Geometrical parameter	Value
1	Inner diameter of the agitated vessel	$D=0.3$ m
2	Height of the liquid in the vessel	$H=2D$
3	Number of baffles	$J=4$
4	Width of baffle	$B=0.1D$
5	Number of impellers	$i=2$ or 1
6	Diameter of the impeller	$d=0.33D$
7	Number of impeller blades	$Z=6$
8	Length of the impeller blade	$a=0.25d$
9	Height of the impeller blade	$b=0.2d$
10	Distance between lower impeller and bottom of the vessel	$h_1=0.33D$
11	Distance between upper impeller and bottom of the vessel	$h_2=0.67D$
12	Distance between gas sparger and bottom of the vessel	$e=0.5h_1$

Sketch of the local heat flux meter is given in Fig. 6. Basic parts of the device, a measuring rod (1) of diameter $2R_1=0.02$ m and a conical sleeve (2) of diameter $2R=0.06$ m were made of stainless steel. Two thermocouples nickel–nichrome (Ni–NiCr) (3) were inserted into the holes of the measuring rod (1). The narrow air-gap of the thickness "c" between parts (1) and (2) was made in order to insulate the element (1), additionally. The chambers (5) and (6) shaped in the flanged housing (4) were fed by a steam via pipe (10) and a condensate was carried off continuously into a condenser pot by means of the stub pipes (8) and (9).

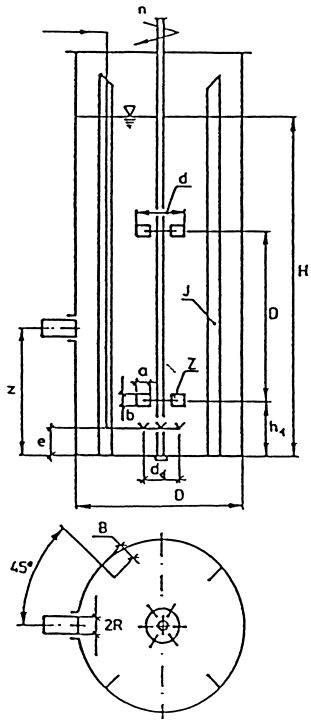

Fig. 4. Geometrical parameters of the agitated vessel used in the study.

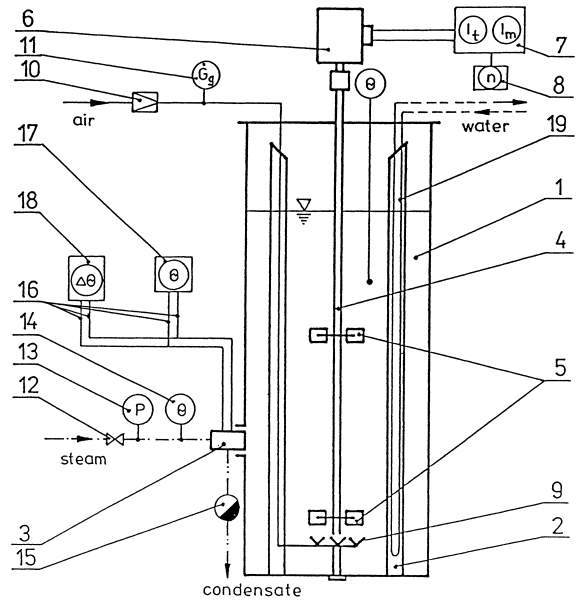

Fig. 5. Experimental set-up. (1) Agitated vessel, (2) baffle, (3) local heat flux meter, (4) shaft, (5) disc turbine, (6) electric motor, (7) steering unit, (8) electronic counter, (9) gas sparger, (10) control valve, (11) rotameter, (12) valve, (13) manometer, (14) thermometer, (15) condenser pot, (16) thermocouples, (17) thermostat, (18) point recorder.

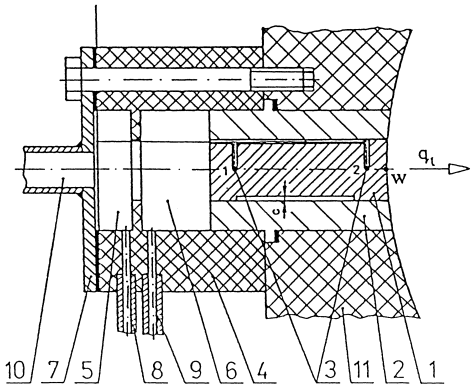

Fig. 6. Local heat flux meter. (1) Measuring element, (2) conical sleeve, (3) thermocouples, (4) flanged housing, (5), (6) heating chambers, (7) metal cover, (8), (9) stub pipe of condensate, (10) stub pipe of steam, and (11) wall of the agitated vessel.

As the steam is used to the heating of the local source then it is possible to obtain relatively large values of the heat flux q_w (approximately 10^5–2×10^5 W m^{-2}) and large, easy to measure, differences of temperature, in consequence.

The measurement of the local heat transfer coefficient α_l by means of the local heat flux meter is based on the indirect evaluation of the heat flux q_w and driving difference of temperature ΔT_l between outer wall of the measuring element T_w and mixed fluid T_m

$$\alpha_l = \frac{q_w}{\Delta T_l} = \frac{q_w}{T_w - T_m}. \tag{17}$$

Heat flux q_w at steady-state conditions can be estimated from the following equations:

$$q_1 = \frac{\lambda}{l_1}(T_1 - T_2), \tag{18}$$

$$q_2 = \frac{\lambda}{l_2}(T_1 - T_w), \tag{19}$$

where

$$q_1 = q_2 = q_w, \tag{20}$$

l_1 is the distance between points 1 and 2, and l_2 is the distance between points 1 and "w" of the measuring element.

Wall temperature T_w can be calculated from Eq. (21) obtained as a result of the rearrangement of Eqs. (18) and (19)

$$T_w = T_1\left[1 - \left(\frac{l_2}{l_1}\right)\right] + \left(\frac{l_2}{l_1}\right)T_2. \tag{21}$$

The measurements were carried out for distilled water and air as a gas phase.

4. Results and discussion

The distributions of the heat transfer coefficient along the wall of the agitated vessel were obtained on the basis of the experimental data. Some results are presented graphically in the form of a function α_l=f(z/H), where coordinate z denotes a distance between measuring point and the bottom of the vessel. The data for distilled water (without gas, w_{og}=0) at different impeller speeds n are shown in Fig. 7. Experimental profiles in the graph have two local maxima in the region of the agitator, where heat transfer is the most intensive. Moreover, the course of these profiles shows that heat transfer coefficient increases with the increase of the impeller speeds.

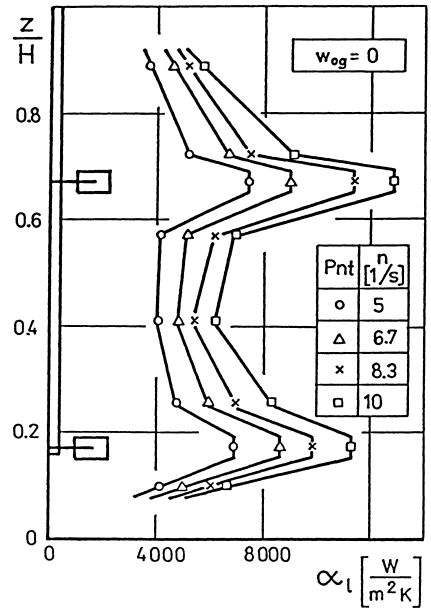

Fig. 7. The profiles α_l=f(z/H) for distilled water (w_{og}=0).

Analogous distributions of the heat transfer coefficient for air–distilled water system at superficial gas velocity $w_{og}=5.1\times10^{-3}$ m s^{-1} is illustrated in Fig. 8. From comparison of the data in Figs. 7 and 8, it can be stated that a value of the heat transfer coefficient for gas–liquid system decreases in the region of the agitator with the increase of the gas flow rate.

Experimental results for slender agitated vessel (H/D=2) equipped with one disc turbine only are shown in Figs. 9 and 10. Comparison of the distributions of the heat transfer coefficient in Figs. 7 and 9, obtained for distilled water (w_{og}=0), proves that the using of two agitators in the slender agitated vessel is reasonable because the intensification of heat transfer process occurs in the region above lower disc turbine. Moreover, the increase of maximum value of α_l is observed in this zone, since the circulation of fluid in upper circulating loop is advantageously modified by the second impeller.

As it can be seen in Figs. 9 and 10, the gas bubbles cause a decrease of the maximum values of the coefficient α_l within the range of the geometrical parameter z/H<0.5. The reason why the agitation is not intensive in the zone above disc turbine (z/H>0.5), especially, in its upper parts, has been being lower position of the single impeller in the slender

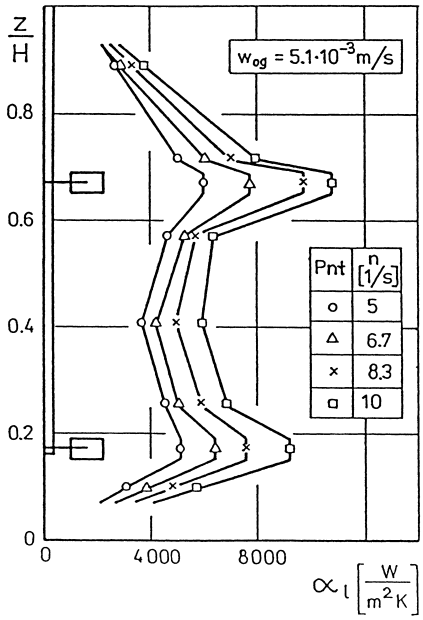

Fig. 8. The profiles $\alpha_l = f(z/H)$ for air–distilled water system ($w_{og}=5.1\times 10^{-3}$ m s^{-1}).

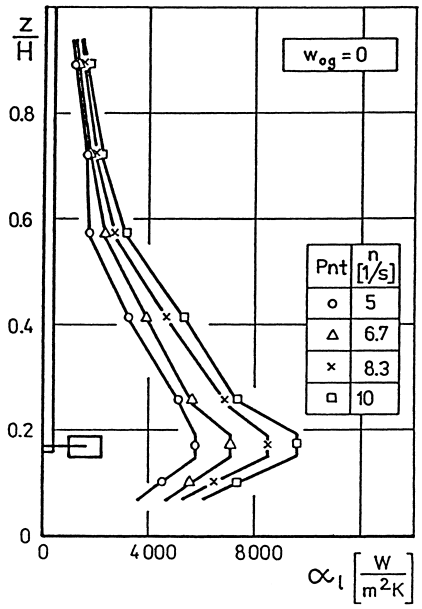

Fig. 9. The profiles $\alpha_l = f(z/H)$ for distilled water ($w_{og}=0$); single disc turbine.

vessel. Therefore, a gas flowing in this zone rapidly intensifies a process of heat transfer at boundary layer of the wall of the agitated vessel. As Fig. 10 shows, the intensification of the heat transfer does not depend on the agitator speed within the range of the geometrical parameter $z/H \geq 0.6$.

An analysis of the experimental data for system of air–distilled water presented in Figs. 8 and 10 has proved that the adding second impeller into the slender agitated vessel has been necessary to reach the increase of the maximum

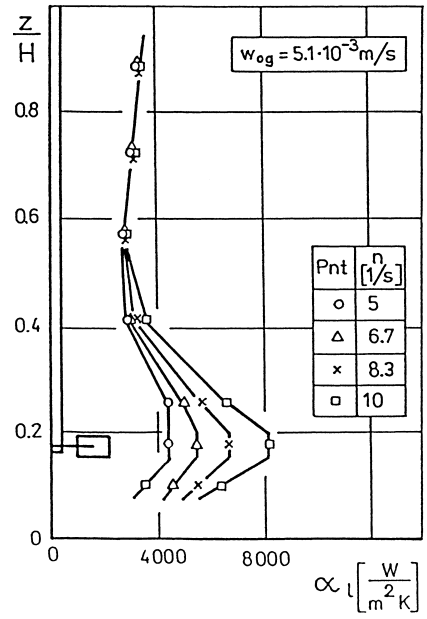

Fig. 10. The profiles $\alpha_l = f(z/H)$ for air–distilled water system ($w_{og}=5.1\times 10^{-3}$ m s^{-1}); single disc turbine.

value of the coefficient α_l and the intensification of the heat transfer coefficient in the zone above the agitator.

The effect of the gas phase on the distribution of the heat transfer coefficient can be estimated from comparison of the experimental profiles of the function $\alpha_l = f(z/H)$ plotted for different values of the superficial gas velocity w_{og} and constant value of the impeller speed n. As Fig. 11 shows, the presence of the gas in the system air–distilled water affects the decrease of the local heat transfer coefficient

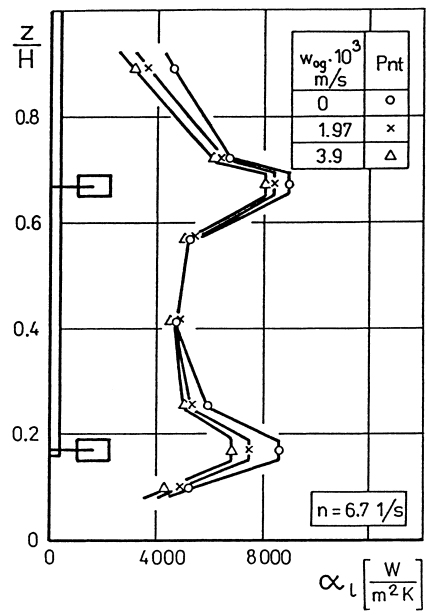

Fig. 11. The profiles $\alpha_l = f(z/H)$ for air–distilled water system; n=6.7 1 s^{-1}.

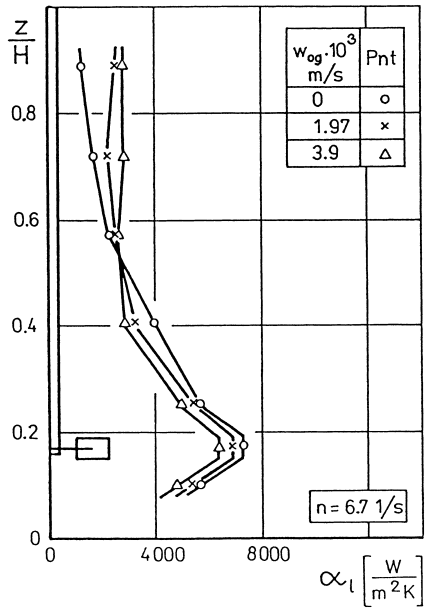

Fig. 12. The profiles $\alpha_l=f(z/H)$ for air–distilled water system; n=6.7 1 s^{-1}; single disc turbine.

along the wall of the agitated vessel, especially, in the region of the lower impeller.

The distributions of the heat transfer coefficient along the wall of the agitated vessel equipped with single disc turbine only are presented in Fig. 12 for air–distilled water system. The dual effect of the gas phase on the heat transfer process appears in such system. The decrease of the coefficient α_l is observed within the range of the geometrical parameter z/H<0.6, whereas the values of the α_l increase for z/H>0.6.

Local heat transfer coefficient α_l for gas–liquid system can be expressed in the form of the dimensionless equation

$$Nu_l = \frac{\alpha_l D}{\lambda} = C_l Re^{A_l} Pr^B Vi^E f_1\left(\frac{z}{H}\right) f_2(w_{og}), \quad (22)$$

where $f_1(z/H)$ and $f_2(w_{og})$ denote dimensionless functions whereas physical parameters of the continuous phase are used for the definitions of the dimensionless numbers Nu_l, Re, Pr and Vi.

The effect of the impeller speeds n on the local coefficient α_l was estimated, analysing the exponent A_l in the equation

$$\frac{Nu_l}{Pr^{0.33} Vi^{0.14}} = C_l\left(\frac{z}{H}, w_{og}\right) Re^{A_l}, \quad (23)$$

where exponents B=0.33 and E=0.14 were assumed on the basis of the literature data [17]. The sets of the experimental data for eight different positions z of the heat flux meter at the vessel wall and five different superficial gas velocities w_{og} were analysed. The results of the A_l for a given value of the w_{og} (w_{og}=const) were averaged numerically using trapezoidal rule in order to determine the mean exponent A for the whole wall of the agitated vessel. Finally, the value A=0.668±0.015 was obtained. The exponent A is in agreement with the literature data [17] for the turbulent regime of

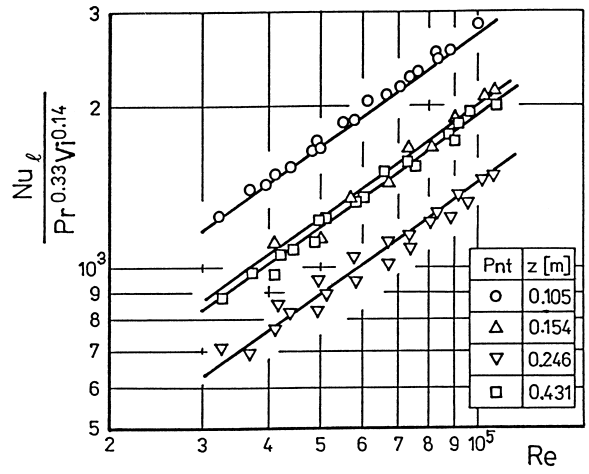

Fig. 13. The dependence $Nu_l/Pr^{0.33}\ Vi^{0.14}=f(Re)$ for different positions z of the heat flux meter; distilled water; w_{og}=0; two disc turbines.

the fluid flow in the standard agitated vessel equipped with baffles and Rushton disc turbine. Some experimental dependencies $Nu_l/Pr^{0.33}Vi^{0.14}$=f(Re) for different positions z of the heat flux meter and different fluids systems are presented in Figs. 13 and 14. Solid lines in these figures correspond to Eq. (23) in which an exponent $A_l=A$=0.67 was assumed. Comparison of the experimental and calculated values in Figs. 13 and 14 shows that Eq. (23) describes the results of the measurements with sufficient accuracy.

Distribution of the heat transfer coefficient α_l along the whole wall of the agitated vessel, i.e. within the range of the geometrical parameter $z/H\langle 0;\ 1\rangle$, was approximated by means of the following equation:

$$Nu_l = \frac{\alpha_l D}{\lambda} = C_l Re^{0.67} Pr^{0.33} Vi^{0.14} f, \quad (24)$$

where $f=f_1f_2$ depends on the variables z/H and w_{og}. Eq. (24)

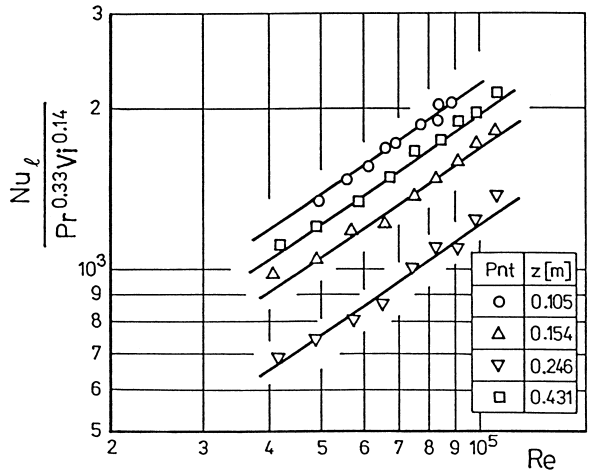

Fig. 14. The dependence $Nu_l/Pr^{0.33}\ Vi^{0.14}$=f($Re$) for different positions z of the heat flux meter; air–distilled water system; $w_{og}=5.1\times10^{-3}$ m s^{-1}; two disc turbines.

Table 2
Constant C_1 and functions $f_1 f_2$ in Eqs. (25)–(30) for air–distilled water system and agitated vessel equipped with two disc turbines; $H/D=2$

No.	z/H	$Nu_l/Re^{0.67}Pr^{0.33}Vi^{0.14}=C_1 f_1 f_2$	
1	$\langle 0;\ 0.15)$	$22.97\left(\frac{z}{H}+0.5\right)^{6.77}\exp\left[-542\left(\frac{z}{H}\right)^{0.92}Fr_g^{0.5}\right]$	(25)
2	$\langle 0.15;\ 0.183\rangle$	$1.24\left(\frac{z}{H}\right)^{0}(1-82.28Fr_g^{0.5})=1.24(1-82.28Fr_g^{0.5})$	(26)
3	$(0.183;\ 0.5\rangle$	$0.1893\left(\frac{z}{H}\right)^{-1.78}\left[2.7287\left(\frac{z}{H}\right)^{2}+0.3187\left(\frac{z}{H}\right)+0.1585\right]\times\exp\left[-15.34\left(\frac{z}{H}\right)^{-1.27}Fr_g^{0.5}\right]$	(27)
4	$(0.5;\ 0.65)$	$6.95\left(\frac{z}{H}\right)^{3.42}\left[37\left(\frac{z}{H}\right)^{2}-43.76\left(\frac{z}{H}\right)+13.63\right]\times\exp\left[\left(-3238.29\left(\frac{z}{H}\right)^{2}+3466.71\left(\frac{z}{H}\right)-924.52\right)Fr_g^{0.5}\right]$	(28)
5	$\langle 0.65;\ 0.683\rangle$	$1.30\left(\frac{z}{H}\right)^{0}(1-50.66Fr_g^{0.5})=1.30(1-50.66Fr_g^{0.5}]$	(29)
6	$(0.683;\ 1\rangle$	$0.2581\left(\frac{z}{H}\right)^{-7.63}\left[17.51\left(\frac{z}{H}\right)^{2}-24.12\left(\frac{z}{H}\right)+8.57\right]\times\exp\left[\left(-8916.1\left(\frac{z}{H}\right)^{2}+13606.26\left(\frac{z}{H}\right)-5172.83\right)Fr_g^{0.5}\right]$	(30)

for the slender agitated vessel equipped with two Rushton disc turbines is presented in Table 2, where Eqs. (25) and (30) for a given range of the parameter z/H are shown, in detail. Eqs. (25) and (30) approximate the results of the measurements with the mean relative error ±4%, within the range of the dimensionless groups variability as follows $Re\in\langle 4\times10^4; 10^5\rangle$, $Fr_g\in\langle 0; 8.8\times10^{-6}\rangle$ and $z/H\in\langle 0; 1\rangle$. As it is seen in Table 2 the function $f_1=f_1(z/H)$ is expressed as the exponential monomial or the result of the multiplication of this monomial and trinomial square. Moreover, the function $f_1(z/H)=1$ for the region of the impellers. The function f_2 has the more complicated form because, except the region of the impellers, depends on the modified Froude number Fr_g (where $Fr_g=w_{og}^2/Dg$), as well as, on the geometrical parameter z/H.

Profiles of the heat transfer coefficient for different superficial gas velocities w_{og}, calculated on the basis of the results of the experiments and Eqs. (25) and (30), are shown in Fig. 15 in the form of the dimensionless function $C_1f_1f_2=Nu_1/Re^{0.67}Pr^{0.33}Vi^{0.14}=f(z/H)$. The results in Fig. 15 confirm that Eqs. (25) and (30) approximate experimental data with sufficient accuracy.

Integrating Eqs. (25) and (30) according to the definition

$$C=\frac{1}{b-a}\int_a^b \frac{Nu_1}{Re^{0.67}Pr^{0.33}Vi^{0.14}}d\left(\frac{z}{H}\right)=\int_a^b C_1f_1f_2d\left(\frac{z}{H}\right)$$

$$=\int_0^1 C_1f_1f_2d\left(\frac{z}{H}\right), \qquad (31)$$

where $a=z/H=0$ and $b=z/H=1$, mean value of the constant C can be determined within the range of the geometrical parameter $z/H\in\langle 0; 1\rangle$. The definition (31) is based on the assumption, that the dependency of the dimensionless numbers everywhere in the vessel content on the local heat transfer coefficient is the same. For example, calculating the integral (31) for liquid (i.e. assuming $w_{og}=0$) agitated in the slender vessel ($H/D=2$) equipped with two Rushton turbines, the value $C=0.769$ was obtained, then

$$Nu=\frac{\alpha D}{\lambda}=0.769Re^{0.67}Pr^{0.33}Vi^{0.14}. \qquad (32)$$

Constant $C=0.769$ in Eq. (32) is in agreement with the literature data $C=0.76$ proposed by Stręk [17] for the standard jacketed agitated vessel ($H/D=1$) equipped with baffles and Rushton disc turbine. The value $C=0.67$ was obtained from analogous calculations for gas–liquid system and $Fr_g=8.8\times10^{-6}$. Therefore within the range of the performed studies, heat transfer coefficient in such system decreases about 12% in comparison with the results for liquid phase.

The results of the experiments, described by means of Eqs. (25) and (30), show the same general trends that Haam et al. [6] found for the case of single impeller. However, inner diameter D of the vessel, a shape of the vessel bottom, number of impellers and a range of the dimensionless number w_0/nd ($w_0/nd\in\langle 5\times10^{-3}; 10^{-2}\rangle$ in this work and $w_0/nd\in\langle 3\times10^{-3}; 10^{-1}\rangle$ in [6]) were different in both experimental systems, therefore heat transfer coefficients obtained can be compared approximately only.

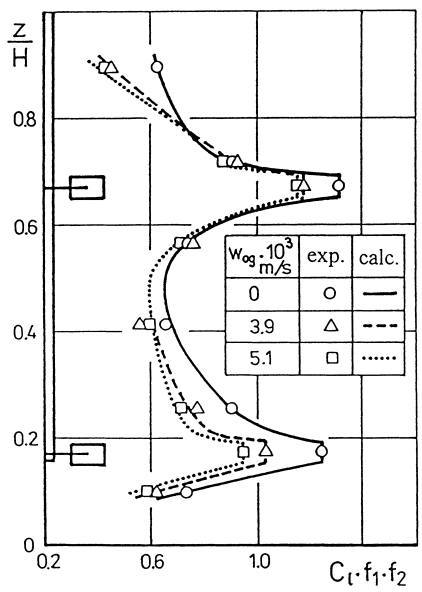

Fig. 15. Comparison of the functions $C_1f_1f_2=f(z/H)$ for air–distilled water system and two disc turbines, calculated from Eqs. (25)–(30)) and experimentally obtained.

5. Conclusions

The experimental distributions of the heat transfer coefficient along the wall of the slender agitated vessel equipped with two disc turbines are found to be useful in practice. The perturbations in the course of the technological processes as a result of a superheating of the vessel wall can be explained on the basis of these profiles.

The results of the experiments have revealed that

- the greatest intensity of the heat transfer occurs in the regions of the agitators, therefore, the location of the short jacket or coil is particularly advantageous in these zones
- heat transfer coefficient decreases with the increase of the gas flow rate in the agitated vessel
- the axial distribution of the heat transfer coefficient can be described by Eqs. (25) and (30).

6. Nomenclature

A	mean value of exponent
A_1	exponent in Eq. (22)
a	thermal diffusivity ($m^2\,s^{-1}$)
a	length of impeller blade (m)
B	baffle width (m)

B, E exponents in Eq. (22)
b width of impeller blade (m)
C constant in Eq. (31)
C_1 constant in Eq. (22)
C_p specific heat (J kg^{-1} K^{-1})
D inner diameter of the agitated vessel (m)
d impeller diameter (m)
d_d diameter of the gas sparger (m)
e distance between gas sparger and bottom of the vessel (m)
F heat transfer surface area (m^2)
f function ($=f_1 f_2$) in Eq. (24))
g acceleration due to gravity (m s^{-2})
H liquid height in the vessel (m)
h_1 distance between disc of the lower impeller and bottom of the vessel (m)
h_2 distance between disc of the upper impeller and bottom of the vessel (m)
i number of impellers
J number of baffles
l distance, meaning of (m) in Eqs. (18) and (19)
n impeller speed (s^{-1})
p correction factor
Q_1 heat rate (W)
q_w heat flux (W m^{-2})
R radius of measuring element (m)
T temperature (K)
V'_g gas flow rate (m^3 s^{-1})
w_{og} superficial gas velocity ($=4V'_g/\pi D^2$) (m s^{-1})
w_z axial velocity (m s^{-1})
y coordinate, perpendicular to the agitated vessel wall (m)
Z number of blades of the impeller
z axial coordinate (m)
z distance between measuring point and bottom of the vessel (m)

Greek letters

α mean heat transfer coefficient (W m^{-2} K^{-1})
α_1 local heat transfer coefficient (W m^{-2} K^{-1})
γ shear rate (s^{-1})
Δ difference
δ_t thermal laminar boundary layer (m)
η dynamic viscosity of liquid (kg m^{-1} s^{-1})
λ thermal conductivity (W m^{-1} K^{-1})
ν kinematic viscosity of liquid (m s^{-2})
ρ density of liquid (kg m^{-3})

Dimensionless numbers

$$Fr_g = \frac{w_{og}^2}{D_g}$$

$$Nu = \frac{\alpha D}{\lambda}$$

$$Nu_1 = \frac{\alpha_1 D}{\lambda}$$

$$Pr = \frac{C_p \eta}{\lambda}$$

$$Re = \frac{nd^2\rho}{\eta}$$

$$Vi = \frac{\eta}{\eta_w}$$

Indices

l local value
w referred to the wall

References

[1] H. Akse, W.J. Beek, F.C.A.A. Van Berkel, J. De Graauw, The local heat transfer at the wall of a large vessel agitated by turbine impellers, Chem. Eng. Sci. 22 (1967) 135–146.
[2] J.R. Bourne, O. Dossenbach, T. Post, Local and average mass and heat transfer generated by Pfaudler-type impellers, Inst. Chem. Eng. Symp. Ser. 89 (1984) 177–191.
[3] J.R. Bourne, O. Dossenbach, T. Post, Local and average mass and heat transfer due to turbine impellers, Fifth European Conference on Mixing, Wuerzburg, BHRA Fluid Engineering, Cranfield, Paper 21, 1985.
[4] J.B. Fasano, R.S. Brodkey, S.J. Haam, Local wall heat transfer coefficients using surface calorimeters, Proceedings of the Seventh European Conference on Mixing, Brugge, Part I, Koninlijke Vlaamse Ingenieursvereniging, 1991, pp. 497–505.
[5] I. Fort, J. Placek, F. Stręk, Z. Jaworski, J. Karcz, Heat and momentum transfer in the wall region of a cylindrical vessel mixed by a turbine impeller, Collect. Czech. Chem. Commun. 44 (1979) 684–699.
[6] S.J. Haam, R.S. Brodkey, J.B. Fasano, Multiphase local heat transfer in a mixing vessel, AIChE Symp. Ser. 286(88) (1992) 93–97.
[7] S. Haam, R.S. Brodkey, J.B. Fasano, Local heat transfer in a mixing vessel using heat flux sensors, Ind. Eng. Chem. Res. 31 (1992) 1384–1391.
[8] S. Haam, R.S. Brodkey, J.B. Fasano, Local heat transfer in a mixing vessel using a high-efficiency impeller, Ind. Eng. Chem. Res. 32 (1993) 575–576.
[9] J. Karcz, Theoretical and experimental analysis of the heat transfer in gas–liquid system for stirred tank equipped with two stirrers on the shaft (in Polish), Pr. Nauk Politechn. Szczecin 447(29) (1991) 1–168.
[10] J. Karcz, F. Stręk, Heat transfer in mechanically stirred gas–liquid system, Proceedings of the Seventh European Conference on Mixing, Brugge, Part I, Koninlijke Vlaamse Ingenieursvereniging, 1991, pp. 251–259.
[11] P. Kurpiers, A. Steiff, P.M. Weinspach, Zum Waermeuebergang und zur Massstabsuebertagung in geruehrten Ein- und Mehrphasenreaktoren mit eingetauchten Heizelementen, Chem. Ing. Techn. 57 (1985) 632–633.
[12] P. Kurpiers, A. Steiff, P.M. Weinspach, Heat transfer and scale-up in stirred single and multiphase reactors with immersed heating elements, Ger. Chem. Eng. 8 (1985) 267–271.
[13] W.M. Lu, C.M. Lan, H.W. Fang, Local heat transfer in a stirred vessel with and without aeration, J. Chem. Eng. Jpn. 28 (1995) 666–672.

[14] K.L. Man, A study of local heat transfer coefficients in mechanically agitated gas–liquid vessels, Fifth European Conference on Mixing, Wuerzburg, BHRA Fluid Engineering, Cranfield, Paper 23, 1985.
[15] K.L. Man, M.F. Edwards, G.T. Polley, A study of local heat transfer coefficients in agitated vessels, Inst. Chem. Eng. Symp. Ser. 89 (1984) 193–207.
[16] B. Platzer, G. Noll, Modellierung des oertlichen ruehrgutseitigen Waermeuebergangs in bewehrten Ruehrkesseln, Chem. Techn. 35 (1983) 140–144.
[17] F. Stręk, Heat transfer in liquid mixers, Intern. Chem. Eng. 3 (1963) 533–556.
[18] F. Stręk, Z. Jaworski, J. Karcz, A study of distributions of the heat transfer coefficient at the wall of the agitated vessel (in Polish), Inz. Chem. i Proc. 1 (1980) 841–858.
[19] F. Stręk, J. Karcz, W. Góra, Patent RP 153 129 (1986).
[20] F. Stręk, J. Karcz, M. Kaznowska, Experimental studies of heat transfer in a liquid phase and gas–liquid system for bottom of a stirred tank, IChEME Symp. Ser. 136 (1994) 407–414.